IET Image Processing

Research Article

Texture spectral similarity criteria

ISSN 1751-9659
Received on 1st March 2019
Revised 9th May 2019
Accepted on 2nd June 2019
doi: 10.1049/iet-ipr.2019.0250
www.ietdl.org

Michal Havlíček[1] ✉, *Michal Haindl*[1]

[1]*Pattern Recognition Department, The Institute of Information Theory and Automation of the Czech Academy of Sciences, 182 08 Prague, Czech Republic*

✉ *E-mail: havlimi2@utia.cas.cz*

Abstract: New similarity criteria capable of assessing spectral modelling plausibility of colour, bidirectional texture functions (BTF), and hyperspectral textures are presented. The criteria credibly compare the multi-spectral pixel values of the textures. They simultaneously consider the pixels of similar values and their mutual ratios. It allows support of the optimal modelling or acquisition setup development by comparing the original data with its synthetic simulations. Analytical applications of the criteria can be spectral based texture retrieval or classification. The suggested criteria together with existing alternatives are extensively tested and compared on a wide variety of colour, BTF, and hyperspectral textures. The performance quality of the criteria is examined in a long series of thousands specially designed monotonically degrading experiments, where proposed ones outperform all tested alternatives.

1 Introduction

A fully automatic texture, or more generally image, quality assessment, and mutual-similarity evaluation of two or more of them present a fundamental but still unsolved complex problem. The recent validation of the state-of-the-art image and texture fidelity criteria [1] on the web-based benchmark (http://tfa.utia.cas.cz) has demonstrated that none of published criteria complex wavelet structural similarity metric (CW-SSIM) [2], structural similarity metric 1 (SSIM-1), structural texture similarity metric 2 (STSIM-2), mahalanobis structural similarity metric (STSIM-M) [3], ζ [4]) can be reliably used for this task at all. There is still a pressing need for a reliable criterion to support texture model development, i.e. a comparison of the original texture with a synthesised or reconstructed one for the evaluation of optimal parameter settings of such a model. Such similarity metrics also play an essential role in efficient content-based image retrieval, e.g. from digital libraries, or multimedia databases. Numerous texture analysis approaches based on various textural features were developed and applied for texture categorisation. However, such textural features (e.g. Haralick's features [5], run-length features [6], Laws's filters [7], Gabor features [8], local binary patterns (LBP) [9], and its various modifications. Markovian features [10] etc.) cannot rank textures according to their visual similarity. Except for Markovian features [10], they are not descriptive; thus, they are useful only for binary decision if two mono-spectral textures are identical or not. Surprisingly, already many advanced approaches are limited to mono-spectral images, which is a significant disadvantage as a colour is arguably the most significant visual feature. Fig. 1 illustrates the case when all six textures have the same all mono-spectral textural features but distinct multi-spectral ones such as the Markovian features [10]. Hence, the multi-spectral texture similarity criteria can be naturally applied for texture retrieval; the opposite does not hold because any mono-spectral textural feature-based retrieval will retrieve all Fig. 1 textures as identical.

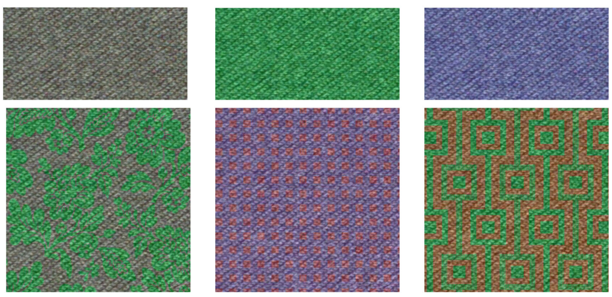

Fig. 1 *Textile textures with distinct multi-spectral but identical mono-spectral textural features*

The psychophysical evaluations [11, 12], i.e. quality assessments performed by humans, currently represent the only reliable option. This approach requires time-demanding experiment design setup, strictly controlled laboratory conditions, and representative sets of testers, i.e. sufficient numbers of individuals, ideally from the public, naive concerning the purpose, and design of the experiment. Such assessing is thus extremely impractical, expensive, generally demanding, and hence non-transferable into daily routine practise, operable on demand, and ideally in real time. Moreover, methods involving human perception are impracticable for hyperspectral data due to the limited tri-chromatic nature of the human vision.

In this paper, the textures or more general images are compared as independent sets of pixels. The pixel values are compared as vectors while the position of the pixels in the textures or images is not considered. This restricted problem will be called in the rest of this paper as a spectral similarity comparison. It deals with the appearance and amount of pixels that occur in only one of the compared images and also the ratio of occurrences of pixels appearing in both images to express their spectral composition difference.

The rest of this paper is organised as follows: Section 2 briefly presents published alternatives to solve the problem of image spectral composition comparison including some based on modifications of techniques developed for slightly different purposes. Section 3 explains in detail our new approach. Section 4 describes the performed criteria validation experiments and used test data. Section 5 shows the achieved results. Section 6 summarises this paper with a discussion and compares our proposed criteria with their existing alternatives.

2 Related work

In this section, we first briefly survey existing methods capable of comparing image spectral composition, and then we show some modifications of existing techniques, initially developed for slightly different use. The symbols ↓ , ↑, or | ↓ | indicate the increasing similarity direction for the corresponding criterion. Most

Table 1 Average evaluation time, on Pentium-2.8 GHz-equivalent CPU, depending on the size of compared images for individual criteria

	8×8	16×16	32×32	64×64
ΔH, $\cap H$, d_{sc}, d_{can}, J, χ^2	0.7 s	0.7 s	0.7 s	0.7 s
EMD	1.8 ms	85.6 ms	5.7 s	7.6 min
$\Delta\mathrm{GCM}_{00}^{111}$	67.0 μs	0.1 ms	0.2 ms	0.5 ms
$d_{\cos}$	32.0 μs	88.0 μs	93.0 μs	0.6 ms
JI, SDI	0.3 ms	4.0 ms	9.0 ms	48.0 ms
rSSIM	31.0 μs	0.1 ms	0.2 ms	1.4 ms
ζ	0.1 ms	2.0 ms	18.0 ms	0.2 s

methods deal with colour images, i.e. three spectral channels only. The straightforward option is to use a three-dimensional (3D) histogram or local histogram [13], which approximates the image colour distribution. Let us denote by a_ϱ and b_ϱ the ϱth bin of the 3D histogram of the images A and B, respectively, where A is the template image and similarly B is the image to be compared. The range of the histogram multi-index $\varrho = i,\ j,\ k$ depends on a colour space C, in which the image is represented, e.g. in case of the standard 24 bit red, green, and blue (RGB) colour space, the range of all three components of the multi-index is an integer from 0 to 255. The most intuitive way is to compute the 3D histograms difference

$$\downarrow \Delta H(A,\ B) = \sum_{\varrho\in C}\left|a_\varrho - b_\varrho\right| \quad \geq 0, \tag{1}$$

which is a special case called block distance, also known as Manhattan distance, of the Minkowski distance

$$\Delta_q H(A,\ B) = \left(\sum_{\varrho\in C}\left|a_\varrho - b_\varrho\right|^q\right)^{1/q}. \tag{2}$$

Furthermore, in practise, frequently used distances based on (2) embrace the Euclidean distance ($q = 2$) or the maximum distance also called Chebyshev distance and known as chessboard distance ($q = \infty$)

$$\Delta_\infty H(A,\ B) = \sum_{\varrho\in C}\max\left\{\left|a_i - b_i\right|,\ \left|a_j - b_j\right|,\ \left|a_k - b_k\right|\right\}, \tag{3}$$

where a_i, a_j, a_k represents first, second, and third components of the vector $\boldsymbol{a}_\rho$ and similarly for b_i, b_j, b_k. Let us mention that for $0 < q < 1$ so-called fractional dissimilarity, the Minkowski distance is not a metric because it violates the triangle inequality [14].

Several other possibilities for 3D histogram comparison have been suggested such as the histogram intersection [15]

$$\downarrow\ \cap H(A,\ B) = 1 - \frac{\sum_{\varrho\in C}\min\left\{a_\rho,\ b_\rho\right\}}{\sum_{\varrho\in C} b_\rho} \geq 0, \tag{4}$$

the squared chord [16]

$$\downarrow d_{sc}(A,\ B) = \sum_{\varrho\in C}\left(\sqrt{a_\varrho} - \sqrt{b_\varrho}\right)^2 \geq 0, \tag{5}$$

and the Canberra metric [16]

$$\downarrow d_{can} = \sum_{C_0}\frac{\left|a_\varrho - b_\varrho\right|}{a_\varrho + b_\varrho} \geq 0, \tag{6}$$

where $C_0 = \left\{\varrho : a_\varrho + b_\varrho \neq 0\right\} \subset C$.

The information theoretic measures can also be considered for evaluating the histogram difference. One possible option is the symmetric modification of the Kullback–Leibler divergence – a variant of the empirical Jeffrey divergence

$$\downarrow J(A,\ B) = \sum_{C^0} a_\varrho \log\frac{2a_\varrho}{a_\varrho + b_\varrho} + b_\varrho \log\frac{2b_\varrho}{a_\varrho + b_\varrho} \geq 0, \tag{7}$$

where $C^0 = \{\varrho : a_\varrho b_\varrho \neq 0\} \subset C$. The Jeffrey divergence is numerically stable, symmetric, and robust concerning noise and the size of histogram bins [17]. Another measure, based on the χ^2 statistic was suggested in [18]

$$\downarrow \chi^2(A,\ B) = \sum_{C_0}\frac{2\left(a_\varrho - \left(\left(a_\varrho + b_\varrho\right)/2\right)\right)^2}{a_\varrho + b_\varrho} \geq 0. \tag{8}$$

Earth Mover's distance (EMD) or Wasserstein [19] is a method to evaluate dissimilarity between two multi-dimensional distributions in some feature space. It is based on the minimal cost that must be paid to transform one distribution into another, where the cost for moving a single feature unit in the feature space is defined by the Euclidean distance, and the total cost is the sum of such single feature moving costs. The measure is formalised as a linear optimisation problem, which makes this method very memorable and especially time-demanding. It turned out that the EMD is inapplicable for the needs of our experiments described and explained in detail in Section 4 as well as for the solution of the problem described in Section 1 as it is limited to unhandily small images (see the comparison of average computing times of individual methods in Table 1). Even its smoothed dual solution [20] is too time-consuming for any practical application which requires the comparison of a more massive amount of pixels.

The generalised colour moments (GCM) [21] suits well to the image spectral composition comparison problem. The GCM of the $(p + q)$th order and the $(\alpha + \beta + \gamma)$th degree is defined as [21]

$$\begin{aligned}\big|\downarrow \big|\Delta\mathrm{GCM}_{pq}^{\alpha\beta\gamma}(A,\ B) \\ = \int\!\!\int_{\langle A\rangle} r_1^p r_2^q [\boldsymbol{Y}^A_{r_1,\ r_2,\ 1}]^\alpha\ [\boldsymbol{Y}^A_{r_1,\ r_2,\ 2}]^\beta\ [\boldsymbol{Y}^A_{r_1,\ r_2,\ 3}]^\gamma\ \mathrm{d}r_1\,\mathrm{d}r_2 \\ - \int\!\!\int_{\langle B\rangle} r_1^p r_2^q [\boldsymbol{Y}^B_{r_1,\ r_2,\ 1}]^\alpha\ [\boldsymbol{Y}^B_{r_1,\ r_2,\ 2}]^\beta\ [\boldsymbol{Y}^B_{r_1,\ r_2,\ 3}]^\gamma\ \mathrm{d}r_1\,\mathrm{d}r_2,\end{aligned} \tag{9}$$

where $r_1,\ r_2 \in \langle A\rangle$ represents planar coordinates of the image pixel $\boldsymbol{Y}^A_r$, $\boldsymbol{Y}^A_{r_1,\ r_2,\ i}$ denotes a pixel intensity in the ith spectral plane of the image A; similarly, $\boldsymbol{Y}^B_{r_1,\ r_2,\ r_3 = i}$, where $r_1,\ r_2 \in \langle B\rangle$. In the case of using GCM for spectral composition comparison, neither of the terms r_1^p and r_2^q is useful, and therefore both might be put equal to one, using those GCMs for which $p = q = 0$ holds. Moreover, it has been observed that the best results are achieved if $\alpha = \beta = \gamma$, specifically using GCMs for $\alpha = \beta = \gamma < 4$. Thus, GCM directly compares image pixels not using their 3D histograms such as methods (1), (4)– (8), similar to the cosine-function-based dissimilarity, which computes an angle between two vectors. Both images A, B must have an identical number of pixels which is a significant drawback of this criterion. This criterion is the only one mentioned in this paper suffering from this. All values of corresponding image spectral channels are arranged into vectors $\boldsymbol{V}_A$ and $\boldsymbol{V}_B$ and the difference is computed as [18, 22]

$$\uparrow d_{\cos}(A,\ B) = \frac{\boldsymbol{V}_A^{\mathrm{T}}\boldsymbol{V}_B}{\parallel V_A \parallel\ \parallel V_B \parallel} \in \langle 0;\ 1\rangle, \tag{10}$$

where $\parallel\quad\parallel$ denotes the vector magnitude.

Different set-theoretic measures can serve as criteria as well. Let sets S_A and S_B denote the sets of unique multi-dimensional vectors representing pixels occurring in the images A and B, respectively. Spectral composition comparison criteria can be based on methods developed for comparing the similarity and diversity of the sample sets such as the Jaccard index (JI) [23]

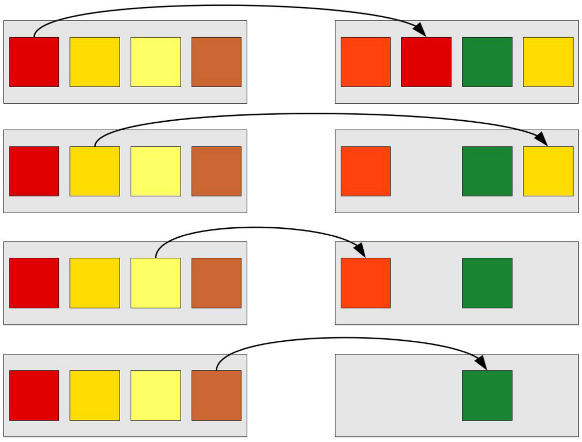

Fig. 2 *Example of the $\zeta(A, B)$ criterion computation comparing two 4 px images. During the evaluation, for every left image pixel the most similar pixel in the right image is found (indicated by arrow) used for the criterion upgrade and labelled as processed*

	1	2	3	4	5	6	7	8
1	0	22.79	27.10	35.31	22.62	48.77	24.86	38.45
2	21.01	0	31.12	39.32	31.77	51.87	31.27	48.01
3	29.86	35.47	0	45.70	17.25	43.66	21.53	45.69
4	32.27	37.54	39.86	0	42.09	32.94	44.28	62.06
5	28.35	35.50	18.14	44.29	0	50.61	14.44	34.20
6	41.95	48.77	39.97	28.04	44.91	0	41.55	56.25
7	29.17	34.90	17.65	47.04	13.20	42.50	0	29.49
8	39.31	50.13	46.52	64.95	34.17	58.66	31.88	0

Fig. 3 *Texture retrieval example. The retrieval results are based on the proposed spectral criterion (16) ($\times 10^4$)*

$$\uparrow \mathrm{JI}(A, B) = \frac{|S_A \cap S_B|}{|S_A \cup S_B|} \in \langle 0; 1 \rangle, \tag{11}$$

or the Sørensen–Dice index (SDI) [24]

$$\uparrow \mathrm{SDI}(A, B) = \frac{2|S_A \cap S_B|}{|S_A| + |S_B|} \in \langle 0; 1 \rangle, \tag{12}$$

where $|.|$ denotes the cardinality of the set. JI and SDI are equivalents in the sense that given a value for SDI, one can calculate the respective JI value and vice versa, using the equations below:

$$\mathrm{JI} = \frac{\mathrm{SDI}}{2 - \mathrm{SDI}}, \tag{13}$$

$$\mathrm{SDI} = \frac{2\mathrm{JI}}{1 + \mathrm{JI}}. \tag{14}$$

Since SDI does not satisfy the triangle inequality, it can be considered a semi-metric version of JI.

Another alternative may be a modified criterion developed for texture comparison as the texture spectral composition comparison might be considered a very special case of this task. It is possible to modify the SSIM [25], for example. SSIM compares local statistics in corresponding sliding windows in two images in either the spatial or wavelet domain. Its form consists of three terms that reflect luminance, contrast, and structure of the textures. In the case of the spectral composition comparison, the structure term is irrelevant so that we define a reduced SSIM

$$\downarrow \mathrm{rSSIM}(A, B) = \frac{1}{\#\{r_3\}} \sum_{\forall r_3} \frac{2\mu_{A, r_3}\mu_{B, r_3}}{\mu^2_{A, r_3} + \mu^2_{B, r_3}} \frac{2\sigma_{A, r_3}\sigma_{B, r_3}}{\sigma^2_{A, r_3} + \sigma^2_{B, r_3}}, \tag{15}$$

where $\#\{r_3\}$ is the spectral index cardinality, i.e. the number of spectral channels μ_{A, r_3} is the mean of r_3th spectral plane of A and σ_{A, r_3} is the standard deviation of r_3th spectral plane of A; similarly, for μ_{B, r_3} and σ_{B, r_3}. $\mathrm{rSSIM}(A, B) = 1$ for spectrally equal textures. The contrast part of (15) is also used in the contrast assessment metric in [26].

The 3D histogram-based criteria (1), (4)–(8) cannot be easily generalised to hyperspectral data, i.e. the data having more than three spectral channels, due to the impossibility of reliably estimating such histograms from limited sample data. GCM (9) could be used for hyperspectral image comparison but the number of multiplication terms to be integrated into (9) significantly increases and so does the range of possible values of the criterion. Set-theoretic measures (11), (12), rSSIM (15), and $d_{\cos}$ (10) criteria can handle the hyperspectral data with no restriction; similarly, as our proposed criterion described in detail in the following section.

3 Proposed approach

We propose a new criterion for image spectral composition comparison. We define the mean exhaustive minimum distance (MEMD)

$$\downarrow \zeta(A, B) = \frac{1}{M} \sum_{(r_1, r_2) \in \langle A \rangle} \min_{(s_1, s_2) \in U} \left\{ \rho\left(\boldsymbol{Y}^A_{r_1, r_2, \bullet}, \boldsymbol{Y}^B_{s_1, s_2, \bullet} \right) \right\} \geq 0, \tag{16}$$

where $\boldsymbol{Y}^A_{r_1, r_2, \bullet}$ represents the pixel at a location (r_1, r_2) in the image A and $\bullet$ denotes all the corresponding spectral indices, and similarly for $\boldsymbol{Y}^B_{s_1, s_2, \bullet}$. Furthermore, ρ is an arbitrary vector metric. We tested, namely Manhattan, Euclidean, and maximum metrics with the last mentioned used obtaining the results in Section 5. U is the set of unprocessed pixel indices of B (illustrated in Fig. 2 and explained in detail below); $M = \min\{\#\{A\}, \#\{B\}\}$; and $\#\{A\}$ is the number of pixels in A, and similarly for $\#\{B\}$. We define $\min\{\varnothing\} = 0$.

The term $\zeta(A, B)$ is evaluated using raster scanning of A. The algorithm scans the pixels of A, from the upper left corner. For each pixel, it searches for the index in the set U for which the corresponding pixel is the closest one, in the sense of the used metric ρ. U contains all spatial indices in the image B at the beginning of the process. When such a pixel is identified at $(s_1, s_2) \in U$, the distance between this pixel and the scanned one from A, measured by ρ, is added to the sum and the index (s_1, s_2) is removed from the set U. The algorithm proceeds to the right bottom of the image A and stops when either all pixels of A are scanned or U becomes an empty set.

The criterion $\zeta(A, B)$ is not symmetrical (Fig. 3) but can be easily symmetrised $\zeta_S(A, B) = 12(\zeta(A, B) + \zeta(B, A))$ if needed. Other analytical properties of (16) are $\zeta(A, B) = 0 \leftrightarrow A = B$ (equality), $\zeta(A, A) = 0$ (reflexivity), $\zeta(A, B) \leq \zeta(A, B')$ for $B' \subset B$ (set cardinality dependence).

Two modifications of the proposed criterion (16), which take into account colour differences just notable by colour psychometric methods in the CIE Lab space, are suggested

$$\downarrow \zeta_2(A, B) = \frac{1}{M} \sum_{(r_1, r_2) \in \langle A \rangle} \kappa(r_1, r_2) \geq 0, \tag{17}$$

$$\kappa(r_1, r_2) = \begin{cases} 1, & \rho^* > 2.3, \\ 0, & \text{otherwise}, \end{cases} \tag{18}$$

$$\rho^* = \min_{(s_1, s_2) \in N} \left\{ \rho^{\text{CIE}}\left(\boldsymbol{Y}^A_{r_1, r_2, \bullet}, \boldsymbol{Y}^B_{s_1, s_2, \bullet} \right) \right\}, \tag{19}$$

where threshold 2.3 was determined in [27] and ρ^{CIE} is the Euclidean distance from the pixel $\boldsymbol{Y}^A_{r_1, r_2, \bullet}$ to pixel $\boldsymbol{Y}^B_{s_1, s_2, \bullet}$ in the CIE Lab colour space [28]. Finally, the last suggested criterion is the weighted average of the just-notable differences

$$\downarrow \zeta_3(A, B) = \frac{1}{M} \sum_{(r_1, r_2) \in A} \kappa(r_1, r_2)\rho^* \geq 0. \tag{20}$$

The terms ζ_2 and ζ_3 are evaluated the same way as the term ζ. Note that the proposed criterion ζ applies to any number of spectral bands, not only for the usual three spectral bands of the standard colour images, while ζ_2 and ζ_3 are derived for the CIE Lab colour space.

4 Comparison

The proposed spectral criteria (16)–(20) together with the previously published alternatives (1), (4)–(15) have been extensively tested on the set of nine controllable degradation experiments described in detail below. The main goal of the performed experiments is to investigate how the individual criteria are affected by the spectral composition changes comparing the image with its modified versions. In the following sections, we describe performed experiments as well as used test data.

4.1 Controlled degradation of the test data

A sequence of gradually degraded textural images is generated from the original test one. The original image serves as the first member of the sequence, i.e. $A^X_1 = A$ and each member, except for the first one, is generated from its predecessor in the sequence as: $A^X_t = f_X\left(A^X_{t-1}\right)$, $t = 1, \ldots, l$, where l equals the length of the sequence and X is the label identifying the experiment (individual experiments described below). Further $\boldsymbol{Y}^A_{r, t}$ denotes the multi-spectral pixel from the experimental image A^X_t at $r = r_1, r_2, r_3$ which is a multi-index with image row, column, and spectral components, respectively. X is the corresponding label of one of the following nine degradation experiments we established for validation tests:

A. Replacing pixel's spectral intensities with the maximal value in the used colour space with the probability $p = (1/l)$

$$\boldsymbol{Y}^A_{r, t} p \leftrightarrow [255, 255, 255]^{\text{T}} \tag{21}$$

Adding a constant $c = (255/l)$ to all pixel's spectral intensities

$$\boldsymbol{Y}^B_{r, t} = \boldsymbol{Y}^B_{r, t-1} + [c, c, c]^{\text{T}} \tag{22}$$

Adding a value depending on the order of the image in the sequence (o) to pixel's spectral intensities

$$\boldsymbol{Y}^{\text{C}}_{r, t} = \boldsymbol{Y}^{\text{C}}_{r, t-1} + [v, v, v]^{\text{T}}, \quad v = \frac{255}{l} \sin\left(\pi \frac{o}{l}\right) \tag{23}$$

Adding a constant $c = (255/l)$ to pixel's spectral intensities and random mutual interchanging with probability $p = 0.5$ with four-connected pixels from $I^{(4)}_r$:

i. $\boldsymbol{Y}^{\text{D}}_{r, t} = \boldsymbol{Y}^{\text{D}}_{r, t-1} + [c, c, c]^{\text{T}}$.

ii. $\boldsymbol{Y}^{\text{D}}_{r, t} p \leftrightarrow \boldsymbol{Y}^{\text{D}}_{s, t}$, $s \in I^{(4)}_r$, $p = 0.5$.

Adding a constant $c = (255/l)$ to pixel's spectral intensities and randomly driven propagating with probability $p = 0.5$ with eight-connected pixels from $I^{(8)}_r$:

i. $\boldsymbol{Y}^{\text{E}}_{r, t} = \boldsymbol{Y}^{\text{E}}_{r, t-1} + [c, c, c]^{\text{T}}$

ii. $\boldsymbol{Y}^{\text{E}}_{s, t} p = \boldsymbol{Y}^{\text{E}}_{r, t}$, $s \in I^{(8)}_r$, $p = 0.5$

Adding a value depending on the order of the image in the sequence (o) to pixel's spectral intensities

$$\boldsymbol{Y}^{\text{F}}_{r, t} = \boldsymbol{Y}^{\text{F}}_{r, t-1} + [o, o, o]^{\text{T}} \tag{24}$$

Adding a pseudo-random vector to each pixel

$$\begin{gathered} \boldsymbol{Y}^{\text{G}}_{r, t} = \boldsymbol{Y}^{\text{G}}_{r, t-1} + [p_1, p_2, p_3]^{\text{T}}, \\ p_1 \simeq N(0, 255), \quad p_2 \simeq N(0, 255), \quad p_3 \simeq N(0, 255) \end{gathered} \tag{25}$$

Blurring the images using the convolution with the 3×3 Gaussian filter

$$\boldsymbol{Y}^{\text{H}}_t = \boldsymbol{Y}^{\text{H}}_{t-1} \times G \quad G = \begin{pmatrix} \frac{1}{16} & \frac{1}{8} & \frac{1}{16} \\ \frac{1}{8} & \frac{1}{4} & \frac{1}{8} \\ \frac{1}{16} & \frac{1}{8} & \frac{1}{16} \end{pmatrix} \tag{26}$$

Adjusting pixel's spectral intensities so as to approach average over spectral channels

$$\boldsymbol{Y}^{\text{I}}_{r, t} = \boldsymbol{Y}^{\text{I}}_{r, t-1} + [k_1, k_2, k_3]^{\text{T}} \tag{27}$$

$$k_i = \begin{cases} 1, & \text{if } \eta > \boldsymbol{Y}_{r_1, r_2, i, t} \\ -1, & \text{if } \eta < \boldsymbol{Y}_{r_1, r_2, i, t} \\ 0, & \text{otherwise} \end{cases} \tag{28}$$

$$\eta = \frac{1}{3} \sum_{r_3 = 1}^{3} \boldsymbol{Y}_{(r_1, r_2, r_3), t}, \tag{29}$$

Several selected members of the degradation sequences generated during the experiments are shown in Fig. 4.

4.2 Evaluation meta-criterion

The tested criteria are applied to quantify spectral composition differences between the template image, i.e. the first member of the degradation sequence and the remaining members. As all those sequences are constructed so that monotone degradation of the original image is guaranteed, i.e. the similarity of the members of the sequence and the original image is decreasing with the order. Good criterion should be able to follow this trend.

The meta-criterion is the number of monotonicity violations of the criterion τ in the experiment X

$$\Xi^{X, \tau} = \sum_{i=1}^{l} 1 - \delta\left(o^X_i - o^{X, \tau}_i\right), \tag{30}$$

where τ is a tested criterion; o^X_i is the rank of a degraded image; $o^{X, \tau}_i$ is its corresponding correct ordering of the τ-criterion-based ranking; and δ is the Kronecker delta function.

4.3 Test data

Our spectral similarity criteria were validated and compared with the alternative measures on three types of visual data – colour, bidirectional texture function (BTF), and hyperspectral textures.

4.3.1 Colour textures: The tested criteria were validated using 250 colour textures of 64×64 px^2 saved as 24 bit RGB portable network graphics (PNG) files (Fig. 5). We selected a wide range of both natural and man-made materials and investigated the applicability of individual criteria. There were several examples for each class of material. All used textures were downloaded from free Internet texture databases [http://texturer.com/.] [http://www.mayang.com/textures/.]. We performed experiments using

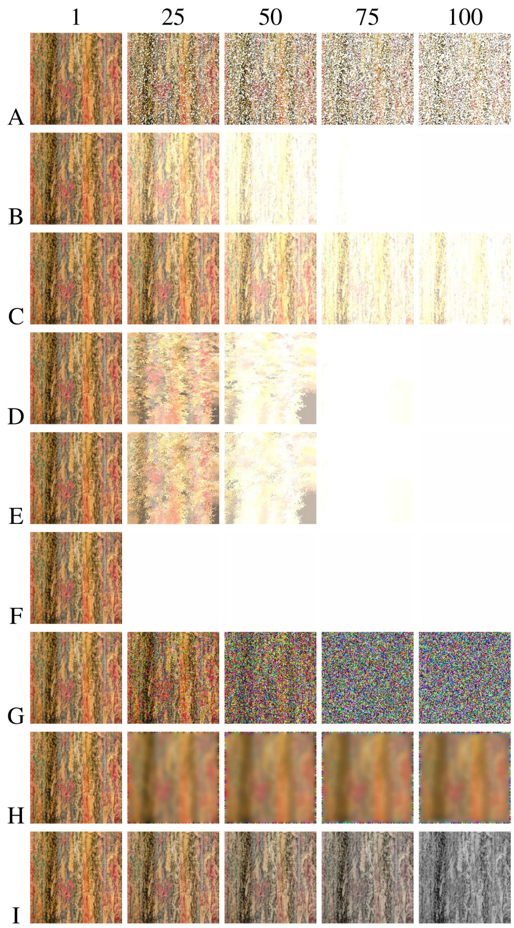

Fig. 4 *Selected degradation sequence members generated during the experiments, A–I top-down. The leftmost column represents the original image, and the degradation intensifies in the rightward direction, where the column number indicates the order of the image in the sequence*

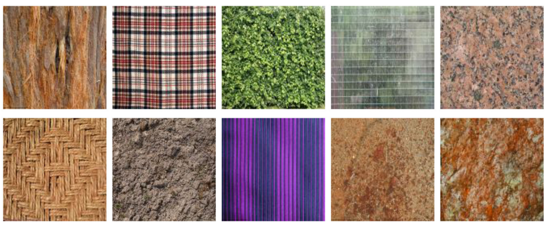

Fig. 5 *Examples of the colour textures used in our experiments*

both original RGB data and their version converted into CIE Lab colour space. The obtained results are presented in Tables 2 and 3 for RGB and in Tables 4 and 5 for CIE Lab.

4.3.2 Bidirectional texture functions: For realistic virtual reality scenes, requiring objects covered with synthetic textures visually as close as possible to real surface materials' appearance are single colour textured mentioned in the previous section unacceptable. Recent most advanced visual representation of such surfaces, BTF [29], which is a 7D function describing the surface appearance variations due to varying spatial position and illumination and viewing angles are the state-of-the-art replacement of static colour textures. A static BTF texture representation requires complex 7D models, which have not yet been developed [11]. Thus, their measurement or mathematical modelling use a BTF space factorisation into a large set of less-dimensional factors. The measured BTF data usually consists of several thousand colour images per material which are analysed for their intrinsic dimensionality [11] and then subsequently approximated by a smaller number of BTF subspaces. It is not possible to run all experiments for all infinite number images, i.e. for any combination of the continuous spherical illumination and viewing angles, of synthetic BTF space texture components. Tested BTF measurements are represented by 20 subspace clusters, which subsequently can serve for building the BTF mathematical model. Subspace cluster were images of 32×32 px^2 saved as 24 bit RGB PNG files. We used ten BTF data sets (one example of the subspace is shown in Fig. 6), and therefore 200 textures were obtained from the University of Bonn database [http://cg.cs.uni-bonn.de/en/projects/btfdbb/download/ubo2003/.] [30]. The achieved results are presented in Tables 6 and 7 for RGB and in Tables 8 and 9 for CIE Lab.

4.3.3 Hyperspectral textures: The hyperspectral textures used for the experiments (Fig. 7) were obtained by taking pictures of the material in 33 different spectral bands spanning from 400 to 720 nm uniformly sampled with a 10 nm step. Each obtained texture of 487×325 px^2 was saved as 33 mono-spectral 16 bit floating-point precision files in OpenEXR format [http://www.openexr.com/.]. We used our measurement of three different materials (plastic foil, fabric, and white foam). Achieved results are presented in Tables 10 and 11 and summarised in section 5.3.

5 Results

In this section, we present and summarise all achieved results during the experiments described in Section 4.1 performed on colour, BTF, and hyperspectral textures and compared and commented on the performance of the criteria. The proposed criterion works well even on non-aligned cutouts from textures as it is illustrated in Fig. 8. Table 12 contains criterion values for all pairs from Fig. 8. The similarity values for texture pairs from

Table 2 Maximal strict monotonicity violation (in per cent) for 250 test colour texture sequences per experiment performed in the RGB colour space, maximum over all experiments, and the rank for the tested criteria

	A	*B*	*C*	*D*	*E*	*F*	*G*	*H*	*I*	Maximum	Rank
ΔH	0	20	17	14	13	6	23	25	19	25	2
$\cap H$	0	20	17	14	13	6	23	25	19	25	2
d_{sc}	0	20	18	19	17	5	23	26	25	26	3
d_{can}	0	47	42	47	47	19	23	35	41	47	7
J	17	33	30	24	25	10	28	35	32	35	5
χ^2	0	22	18	18	17	5	23	26	24	26	3
$\Delta\mathrm{GCM}_{00}^{111}$	0	0	0	4	4	0	29	31	25	31	4
d_{cos}	47	47	46	47	47	21	47	47	47	47	7
JI	22	47	44	46	44	21	38	30	34	47	7
SDI	28	41	40	38	38	19	38	33	33	41	6
rSSIM	47	47	46	47	47	21	47	47	47	47	7
ζ	0	0	1	3	3	0	1	8	5	8	1

Table 3 Average strict monotonicity violation (in per cent) for 250 test colour texture sequences per experiment performed in the RGB colour space, the average over all experiments, and the rank for the tested criteria

	A	*B*	*C*	*D*	*E*	*F*	*G*	*H*	*I*	⊘	Rank
ΔH	0	3	5	3	3	1	13	16	8	6	3
$\cap H$	0	3	5	3	3	1	13	16	8	6	3
d_{sc}	0	3	5	4	4	1	14	17	9	6	3
d_{can}	0	34	29	40	40	12	17	20	31	25	7
J	7	5	9	7	7	3	14	24	14	10	4
χ^2	0	3	5	4	4	1	14	16	9	6	3
$\Delta\mathrm{GCM}_{00}^{111}$	0	0	0	0	0	0	11	9	3	3	2
$d_{\cos}$	29	44	45	31	31	19	47	47	47	38	8
JI	10	8	26	7	7	4	28	24	26	16	5
SDI	16	10	23	9	9	4	28	24	26	17	6
rSSIM	43	44	46	42	42	20	47	25	47	39	9
ζ	0	0	0	0	0	0	0	2	0	0	1

Table 4 Maximal strict monotonicity violation (in per cent) for 250 test colour texture sequences per experiment performed in the CIE Lab colour space, maximum over all experiments, and the rank for the tested criteria

	A	*B*	*C*	*D*	*E*	*F*	*G*	*H*	*I*	Maximum	Rank
ΔH	0	2	4	2	2	2	17	20	16	20	4
$\cap H$	0	2	4	2	2	2	17	20	16	20	4
d_{sc}	0	3	4	3	2	2	19	22	21	22	5
d_{can}	0	20	8	47	47	8	17	23	45	47	9
J	14	3	7	3	3	3	35	42	34	42	7
χ^2	0	3	4	2	2	2	20	22	19	22	5
$\Delta\mathrm{GCM}_{00}^{111}$	0	0	0	0	0	0	16	19	27	27	6
$d_{\cos}$	25	47	46	47	47	21	47	47	47	47	9
JI	6	5	8	5	6	4	43	38	36	43	8
SDI	8	5	7	6	5	3	43	37	35	43	8
rSSIM	47	47	46	47	47	21	47	47	47	47	9
ζ	0	0	0	0	0	0	0	2	0	2	2
ζ_2	0	2	3	2	2	1	15	12	4	15	3
ζ_3	0	0	0	0	0	0	0	1	1	1	1

Table 5 Average strict monotonicity violation (in per cent) for 250 test colour texture sequences per experiment performed in the CIE Lab colour space, the average over all experiments, and the rank for the tested criteria

	A	*B*	*C*	*D*	*E*	*F*	*G*	*H*	*I*	⊘	Rank
ΔH	0	0	0	0	0	0	10	6	2	2	3
$\cap H$	0	0	0	0	0	0	10	6	2	2	3
d_{sc}	0	0	0	0	0	0	12	5	3	2	3
d_{can}	0	14	1	45	45	5	9	4	32	17	7
J	1	1	2	1	1	1	25	25	12	7	4
χ^2	0	0	0	0	0	0	11	5	3	2	3
$\Delta\mathrm{GCM}_{00}^{111}$	0	0	0	0	0	0	5	5	7	2	3
$d_{\cos}$	8	46	45	46	46	21	43	46	46	39	8
JI	1	1	2	1	1	1	37	29	16	10	5
SDI	3	1	2	2	2	1	37	29	18	11	6
rSSIM	46	46	45	46	46	21	46	40	46	42	9
ζ	0	0	0	0	0	0	0	0	0	0	1
ζ_2	0	0	0	0	0	0	8	2	0	1	2
ζ_3	0	0	0	0	0	0	0	0	0	0	1

different textures are the order of magnitude larger than for cutout pairs from the same texture.

5.1 Colour textures

Achieved results of experiments with colour textures in the RGB space are summarised in Tables 2 and 3. It is apparent that both $d_{\cos}$ (10) and rSSIM (15) criteria reached the highest average and maximal error rate, i.e. the percentage of strict monotonicity violation of image differences. With minimal average error of 19% for $d_{\cos}$ 20% for rSSIM during experiment ***F***, those criteria proved to be considerably unreliable and thus inapplicable for colour texture comparison. The criteria JI (11), SDI (12) and *J* (7) achieved similar results which were expected due to their similar definition but they proved to be only slightly more successful than rSSIM and $d_{\cos}$. 3D histogram-based criteria ΔH (1) and $\cap H$ (4) demonstrated the same behaviour, and they scored quite well on average but they failed in experiments G–I. Moreover, their

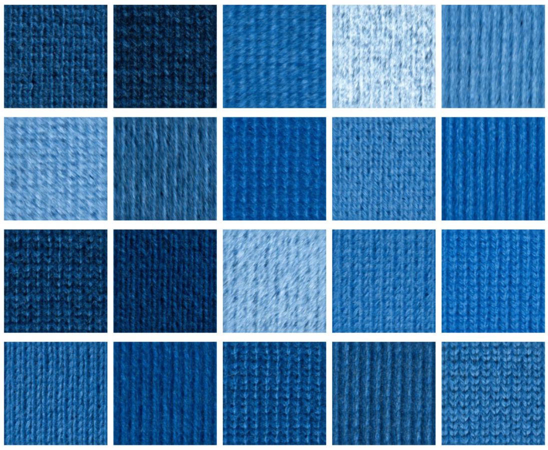

Fig. 6 *Textures representing BTF subspace clusters approximating original BTF data acquired by measuring the wool material. Original data were taken from the BTF database of the University of Bonn [30]. BTF subspace textures were used in our experiments*

Table 6 Maximal strict monotonicity violation (in per cent) for 200 test BTF data sequences per experiment performed in the RGB colour space, maximum over all experiments, and the rank for the tested criteria

	A	*B*	*C*	*D*	*E*	*F*	*G*	*H*	*I*	⊘	Rank
ΔH	0	3	9	4	3	2	16	21	10	21	2
$\cap H$	0	3	9	4	3	2	16	21	10	21	2
d_{sc}	0	3	8	5	5	2	20	23	16	23	3
d_{can}	0	47	41	44	45	18	22	24	40	47	8
J	17	7	8	11	9	5	31	38	27	38	5
χ^2	0	3	8	5	4	2	20	23	15	23	3
$\Delta \mathrm{GCM}_{00}^{111}$	0	0	0	1	0	0	31	33	27	33	4
d_{cos}	47	47	46	47	47	21	47	47	47	47	8
JI	14	15	21	12	14	11	39	33	31	39	6
SDI	20	13	16	12	12	10	40	34	30	40	7
rSSIM	47	47	46	47	47	21	47	47	47	47	8
ζ	0	0	0	0	0	0	2	7	4	7	1

Table 7 Average strict monotonicity violation (in per cent) for 200 test BTF data sequences per experiment performed in RGB colour space, the average over all experiments, and rank for tested criteria

	A	*B*	*C*	*D*	*E*	*F*	*G*	*H*	*I*	⊘	Rank
ΔH	0	0	1	0	0	0	18	13	3	3	2
$\cap H$	0	0	1	0	0	0	18	13	3	3	2
d_{sc}	0	0	1	1	1	0	9	13	4	3	2
d_{can}	0	19	14	34	34	7	14	12	30	18	6
J	7	2	4	2	2	2	9	26	7	7	3
χ^2	0	0	1	1	1	0	9	13	3	3	2
$\Delta \mathrm{GCM}_{00}^{111}$	0	0	0	0	0	0	13	13	3	3	2
d_{cos}	19	40	43	30	30	18	44	46	46	35	7
JI	4	1	3	1	1	1	31	26	21	10	4
SDI	8	2	3	2	2	1	31	26	23	11	5
rSSIM	43	40	44	38	38	18	47	38	45	39	8
ζ	0	0	0	0	0	0	0	1	0	0	1

maximal error rate which reflects a total failure in certain evaluation is too high in all performed experiments, except for experiment A. The criteria d_{sc} (5), d_{can} (6), and χ^2 (8) achieved similar results as the criterion ΔH and the deviation from the results might be caused by rounding errors. The GCM-based criterion (9) failed only in experiments G–I. Our criterion ζ (16) achieved zero average error rate over all experiments as the only tested method with only minor failure in the experiment H scoring with only 2% average, 8% maximal error rate, and zero average and few per cents maximal error rate in the remaining experiments. Tables 4 and 5 present results achieved with the same data transformed from RGB to CIE Lab colour space. It is obvious that the colour space transformation significantly affects the results. 3D histogram-based criteria (except for d_{can}) achieved both lower average and maximal errors in all experiments. Average errors of the remaining criteria are similar to the results obtained using data in the RGB colour space, except for JI and SDI decreasing the average error of about 6%. Criterion ζ achieved zero average error over all experiments again, while decreasing maximal error of about 6% too. This indicates correctness use of ζ for comparison in the sense of colour psychometric methods. The same holds for ζ_3 which was proposed taking into account colour differences just notable by such methods in the CIE Lab space. On the other hand, ζ_2 designed for the same purpose seems to be not so robust resulting with both higher average and maximal error.

5.2 Bidirectional texture functions

The achieved results are summarised in Tables 6 and 7. The behaviours of all tested criteria are similar as in case of colour texture test data (compared with Tables 2 and 3). On the other hand, overall results look better as tested BTF textures were images with lower contrast and overall colourfulness in comparison with the used colour textures. Tables 8 and 9 present results achieved with the same data transformed from RGB to the CIE Lab colour space. The transformation affected the results in a similar way as in

Table 8 Maximal strict monotonicity violation (in per cent) for 200 test BTF texture sequences per experiment performed in CIE Lab colour space, maximal over all experiments, and rank for tested criteria

	A	*B*	*C*	*D*	*E*	*F*	*G*	*H*	*I*	Maximum	Rank
ΔH	0	0	0	0	0	0	18	13	6	18	4
$\cap H$	0	0	0	0	0	0	18	13	6	18	4
d_{sc}	0	0	0	0	0	0	21	12	10	21	5
d_{can}	0	14	5	43	45	6	23	10	40	45	10
J	10	1	3	1	1	1	30	31	29	31	7
χ^2	0	0	0	0	0	0	21	12	7	21	5
ΔGCM_{00}^{111}	0	0	0	0	0	0	15	22	24	24	6
d_{cos}	36	47	46	47	47	21	47	47	47	47	11
JI	3	2	3	2	2	3	41	35	32	41	8
SDI	5	1	3	2	2	2	42	36	24	42	9
rSSIM	47	47	46	47	47	21	47	47	47	47	11
ζ	0	0	0	0	0	0	0	1	1	1	1
ζ_2	0	0	0	0	0	0	16	5	2	16	3
ζ_3	0	0	0	0	0	0	0	1	2	2	2

Table 9 Average strict monotonicity violation (in per cent) for 200 test BTF texture sequences per experiment performed in CIE Lab colour space, the average over all experiments, and rank for tested criteria

	A	*B*	*C*	*D*	*E*	*F*	*G*	*H*	*I*	⊘	Rank
ΔH	0	0	0	0	0	0	10	2	1	1	2
$\cap H$	0	0	0	0	0	0	10	2	1	1	2
d_{sc}	0	0	0	0	0	0	13	2	1	2	3
d_{can}	0	6	0	31	32	3	137	2	26	13	6
J	1	0	1	0	0	0	17	16	5	5	4
χ^2	0	0	0	0	0	0	12	1	1	2	3
ΔGCM_{00}^{111}	0	0	0	0	0	0	2	4	8	1	2
d_{cos}	6	42	41	41	41	19	35	41	42	34	7
JI	0	1	1	1	1	1	32	27	7	8	5
SDI	1	1	1	1	1	1	32	27	9	8	5
rSSIM	42	42	41	41	41	18	42	41	40	39	8
ζ	0	0	0	0	0	0	0	0	0	0	1
ζ_2	0	0	0	0	0	0	8	0	0	1	2
ζ_3	0	0	0	0	0	0	0	0	0	0	1

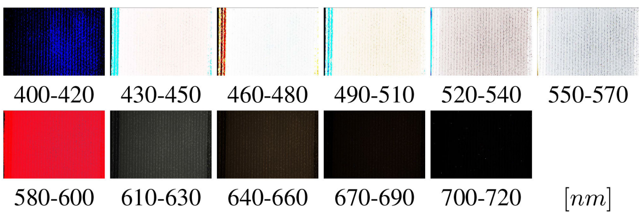

Fig. 7 *Data of the original 33 spectral bands of the hyperspectral texture of the foil grouped into triplets and visualised as RGB images so that individual images represent the texture data acquired in the wavelength range (in nanometre) marked below them*

Table 10 Maximal strict monotonicity violation (in per cent) for three test hyperspectral data sequences per experiment, maximum over all experiments, and the rank for the tested criteria

	A	*B*	*C*	*D*	*E*	*F*	*G*	*H*	*I*	⊘	Rank
ΔGCM_{00}^{111}	0	0	0	0	0	0	0	0	0	0	1
d_{cos}	34	41	42	26	26	17	47	47	47	47	4
JI	0	4	7	6	4	3	25	25	9	25	2
SDI	0	2	4	4	4	2	26	26	16	26	3
rSSIM	38	42	46	30	31	19	47	47	47	47	4
ζ	0	0	0	0	0	0	0	0	0	0	1

Table 11 Average strict monotonicity violation (in per cent) for three test hyperspectral data sequences per experiment, average over all experiments, and the rank for the tested criteria

	A	*B*	*C*	*D*	*E*	*F*	*G*	*H*	*I*	⊘	Rank
$\Delta\mathrm{GCM}_{00}^{111}$	0	0	0	0	0	0	0	0	0	0	1
$d_{\cos}$	30	35	41	21	22	15	47	47	47	34	3
JI	0	3	4	4	3	2	24	24	3	7	2
SDI	0	2	2	3	3	1	25	25	5	7	2
rSSIM	36	38	46	28	28	18	47	25	47	37	4
ζ	0	0	0	0	0	0	0	0	0	0	1

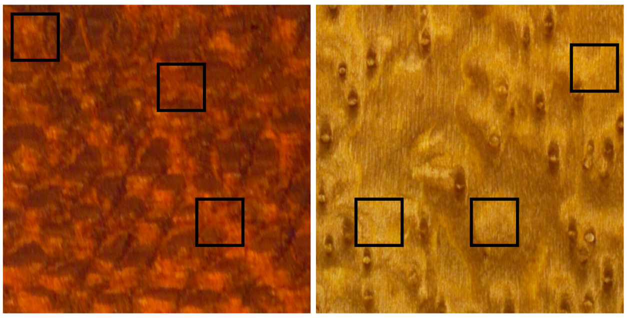

Fig. 8 *Examples of two wood textures with selected cuts (W1-1, W1-2, W1-3, W2-1, W2-2, and W2-3 rightwards) to be compared*

Table 12 Criterion values for all non-align cutout pairs from Fig. 8 ($\times 10^5$)

	W1-1	W1-2	W1-3	W2-1	W2-2	W2-3
W1-1	0	1.87	3.99	27.68	19.59	23.60
W1-2	1.65	0	3.86	28.74	20.63	24.66
W1-3	4.01	3.96	0	25.27	17.18	21.19
W2-1	27.73	28.75	25.35	0	8.27	5.36
W2-2	19.75	20.70	17.28	8.19	0	4.96
W2-3	23.74	24.69	21.27	4.87	5.49	0

	1 	2 	3 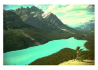	4 	5 
1 	0	400.95	337.65	378.50	455.04
2 	420.96	0	160.97	86.12	140.98
3 	365.79	160.47	0	184.62	239.15
4 	392.88	76.81	178.67	0	117.92
5 	462.80	140.54	221.20	152.28	0

Fig. 9 *Image retrieval example. The retrieval results are based on the proposed spectral criterion (16) ($\times 10^5$)*

the case of colour textures (Section 5.1), though the difference is not so notable.

5.3 Hyperspectral textures

The achieved results are presented in Tables 10 and 11. Again, these results are similar to that achieved during experiments with colour and BTF textures. Surprisingly, the criteria $d_{\cos}$ and rSSIM scored much better in the cases of D and F experiments compared with the results achieved on both colour and BTF data. This might be caused by the overall lower dispersion in hyperspectral data. Similarly, the results of the JI and SDI criteria were better perhaps because there were fewer unique multi-dimensional vectors appearing in the sets. Both GCM and MEMD ζ performed with zero maximal error rate in all experiments.

5.4 Texture and image colour-based retrieval

The last matching matrices Fig. 3 and 9 illustrate possible utilisation of our spectral similarity criterion ζ in a colour-based texture or image retrieval applications. The matrix Fig. 3 shows the most similar textures to be 5, 7, 3, whereas the textures 4 and 6 are distinct from others and slightly related to each other. The biggest spectral difference has textures 4 and 8. Some relative differences, which can be exploited for spectral clustering, are 5, 7–23, 5, 3–28, 5, 4–68, and 4,8–100%. The symmetrised criterion for texture pair (5, 7) $\zeta_S(5, 7) = 13.77$ has also the minimal value, whereas $\zeta_S(4, 8) = 63.51$ is the maximum. Fig. 9 shows the image retrieval application, where images (2, 4) are the most similar and (1, 5) the most distinct. Fig. 10 contains the symmetrised criterion version $\zeta_S(A, B)$. These tables confirm that the criterion, as well as its symmetrised version, lead to the same conclusion.

6 Conclusions

We present new criteria for comparing the spectral similarity of the colour, BTFs, and hyperspectral textures or images. This comparison represents a partial solution for assessing the quality of the multi-spectral textured images and also for the most advanced visual representation of material surfaces – the BTF. The proposed criteria simultaneously consider texture spectral similarity as well as the mutual ratios of similar pixels.

Although the criteria do not consider the positions of the pixels in the images, they can assist in numerous texture-analytic or synthesis applications. The performance quality of the proposed criteria is demonstrated on the extensive series of 407,700 specially designed monotonically image degrading experiments, which also serve for the comparison with the existing alternative methods. Unlike many existing approaches (1), (4)– (8), the MEMD criterion ζ (16) is not based on 3D histograms, instead of representing the estimate of the image spectral distribution, and requiring a

	1 	2 	3 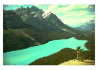	4 	5 
1 	0				
2 	410.96	0			
3 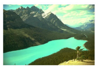	351.72	160.72	0		
4 	385.69	81.47	181.65	0	
5 	458.92	140.76	230.18	135.10	0

Fig. 10 *Image retrieval example based on the proposed symmetrised (ζ_S) spectral criterion* ($\times 10^5$)

sufficiently large data set, which is seldom available. The criterion (16) has no limit on the number of spectral bands. The proposed criteria can be exploited in simple spectral based texture or image retrieval or (un)supervised classification methods.

On the other hand, the MEMD criterion ζ and its perception motivated variants (17) and (20) are slightly more time-demanding than some alternative criteria, except for EMD, which is both more time- and memory-demanding in such a way that it is practically unusable for our purposes. The presented criteria propose a reliable fully automatic alternative to psychophysical experiments, which are, moreover, extremely impractical due to their cost and strict demands on design setup, conditions control, human resources, and time. Additionally, psychophysical experiments are restricted to visualise maximally 3D data which is due to the limited tri-chromatic nature of the human vision. The proposed criteria have entirely outperformed all compared (11 and 5 in case of hyperspectral data) tested alternative criteria in our nearly half a million experiments.

7 Acknowledgment

This research was supported by the Czech Science Foundation project GAČR 14-12340S.

8 References

[1] Haindl, M., Kudělka, M.J.: 'Texture fidelity benchmark'. 2014 Int. Workshop on Computational Intelligence for Multimedia Understanding (IWCIM), Paris, France, 2014, pp. 1–5. Available at http://ieeexplore.ieee.org/stamp/stamp.jsp?tp=arnumber=7008812isnumber=7008791

[2] Wang, Z., Simoncelli, E.P.: 'Translation insensitive image similarity in complex wavelet domain'. IEEE Int. Conf. Acoustics, Speech, and Signal Processing 2005 Proc. (ICASSP 05), Philadelphia, USA, 2005, pp. 573–576

[3] Zujovic, J., Pappas, T.N., Neuhoff, D.L.: 'Structural texture similarity metrics for image analysis and retrieval', *IEEE Trans. Image Process.*, 2013, **22**, (7), pp. 2545–2558

[4] Kudělka, M., Haindl, M.: 'Texture fidelity criterion'. 2016 IEEE Int. Conf. Image Processing (ICIP), Phoenix, USA, 2016, pp. 2062–2066. Available at http://2016.ieeeicip.org/

[5] Haralick, R.M., Shanmugam, K., Dinstein, I.: 'Textural features for image classification', *IEEE Trans. Syst. Man Cybern.*, 1973, **SMC-3**, (6), pp. 610–621

[6] Galloway, M.M.: 'Texture analysis using gray level run lengths', *Comput. Graph. Image Process.*, 1975, **4**, (2), pp. 172–179

[7] Laws, K.I.: 'Rapid texture identification'. Proc. SPIE Conf. Image Processing for Missile Guidance, San Diego, USA, 1980, pp. 376–380

[8] Manjunath, B.S., Ma, W.Y.: 'Texture features for browsing and retrieval of image data', *IEEE Trans. Pattern Anal. Mach. Intell.*, 1996, **18**, (8), pp. 837–842

[9] Ojala, T., Pietikäinen, M., Mäenpää, T.: 'Multiresolution gray-scale and rotation invariant texture classification with local binary patterns', *IEEE Trans. Pattern Anal. Mach. Intell.*, 2002, **24**, (7), pp. 971–987

[10] Haindl, M., Mikeš, S.: 'Unsupervised texture segmentation using multispectral modelling approach'. Proc. 18th Int. Conf. Pattern Recognition ICPR 2006, 2006, vol. **II**, pp. 203–206. Available at http://doi.ieeecomputersociety.org/10.1109/ICPR.2006.1148

[11] Haindl, M., Filip, J.: 'Visual texture', in Singh, S., Kang, S.B. (Eds.): '*Advances in computer vision and pattern recognition*' (Springer-Verlag London, London, 2012)

[12] Viethen, J., van Vessem, T., Goudbeek, M., *et al.*: 'Color in reference production: the role of color similarity and color codability', *Cogn. Sci.*, 2017, **41**, pp. 1493–1514

[13] Yuan, J., Wang, D., Cheriyadat, A.M.: 'Factorization-based texture segmentation', *IEEE Trans. Image Process.*, 2015, **24**, (11), pp. 3488–3497

[14] Howarth, P., Rüger, S.M.: 'Fractional distance measures for content-based image retrieval'. European Conf. Information Retrieval (ECIR), Santiago de Compostela, Spain, 2005 (LNCS, **3408**), pp. 447–456. Available at http://dblp.uni-trier.de/db/conf/ecir/ecir2005.html#HowarthR05

[15] Swain, M.J., Ballard, D.H.: 'Color indexing', *Int. J. Comput. Vis.*, 1991, **7**, (1), pp. 11–32

[16] Kokare, M., Chatterji, B., Biswas, P.: 'Comparison of similarity metrics for texture image retrieval'. TENCON 2003 Conf. Convergent Technologies for the Asia-Pacific Region, Bangalore, India, 2003, vol. **2**, pp. 571–575

[17] Puzicha, J., Hofmann, T., Buhmann, J.M.: 'Non-parametric similarity measures for unsupervised texture segmentation and image retrieval'. Proc. IEEE Int. Conf. Computer Vision and Pattern Recognition, San Juan, Puerto Rico, 1997, pp. 267–272

[18] Zhang, D., Lu, G.: 'Evaluation of similarity measurement for image retrieval'. Proc. 2003 Int. Conf. Neural Networks and Signal Processing, 2003, Nanjing, China, 2003, vol. **2**, pp. 928–931

[19] Rubner, Y., Tomasi, C., Guibas, L.J.: 'The earth mover's distance as a metric for image retrieval', *Int. J. Comput. Vis.*, 2000, **40**, (2), pp. 99–121. Available at http://dx.doi.org/10.1023/A:1026543900054

[20] Cuturi, M., Peyré, G.: 'A smoothed dual approach for variational Wasserstein problems', *SIAM J. Imaging Sci.*, 2016, **9**, (1), pp. 320–343

[21] Mindru, F., Moons, T., Gool, L.V.: 'Color-based moment invariants for viewpoint and illumination independent recognition of planar color patterns'. Illumination Independent Recognition of Planar Color Patterns Proc. ICAPR'98, Rio de Janeiro, Brazil, 1998, pp. 113–122

[22] Moroney, N., Gottwals, M.M., Tasti, I.: 'Generating color similarity measures'. Google Patents, US Patent App. 15/307,349, 2017

[23] Jaccard, P.: '*Etude comparative de la distribution florale dans une portion des Alpes et du Jura*'. (Impr. Corbaz, Basel, Switzerland, 1901)

[24] Dice, L.R.: 'Measures of the amount of ecologic association between species', *Ecology*, 1945, **26**, (3), pp. 297–302

[25] Wang, Z., Bovik, A.C., Sheikh, H.R., *et al.*: 'Image quality assessment: from error visibility to structural similarity', *IEEE Trans. Image Process.*, 2004, **13**, (4), pp. 600–612. Available at http://dx.doi.org/10.1109/TIP.2003.819861

[26] Niu, Y., Zhang, H., Guo, W., *et al.*: 'Image quality assessment for color correction based on color contrast similarity and color value difference', *IEEE Trans. Circuits Syst. Video Technol.*, 2018, **28**, (4), pp. 849–862

[27] Mahy, M., Eycken, L., Oosterlinck, A.: 'Evaluation of uniform color spaces developed after the adoption of CIE Lab and CIE Luv', *Color Res. Appl.*, 1994, **19**, (2), pp. 105–121

[28] Wyszecki, G., Stiles, W.S.: '*Color science*', vol. **8** (Wiley, New York, 1982)

[29] Dana, K.J., Nayar, S.K., van Ginneken, B., *et al.*: 'Reflectance and texture of real-world surfaces'. Computer Vision and Pattern Recognition (CVPR), San Juan, Puerto Rico, 1997, pp. 151–157

[30] Sattler, M., Sarlette, R., Klein, R.: 'Efficient and realistic visualization of cloth'. Eurographics Symp. Rendering 2003, Leuven, Belgium, 2003